Phys. Status Solidi B **249,** No. 10, 1914–1918 (2012) / **DOI** 10.1002/pssb.201200377

Part of Special Issue
Phase-change memory: Science and applications

physica status solidi b
www.pss-b.com
basic solid state physics

# Truncated Lorch-window method revealing the off-octahedral Ge in nanocrystalline $Ge_2Sb_2Te_5$

**X. Q. Liu[*,1], X. B. Li[2], B. Zhang[1], S. B. Zhang[3], E. Ma[4], Z. Zhang[1,5], and X. D. Han[**,1]**

[1] Institute of Microstructure and Property of Advanced Materials, Beijing University of Technology, Beijing 100124, P. R. China
[2] State Key Laboratory on Integrated Optoelectronics College of Electronic Science and Engineering, Jilin University, Changchun 130012, P. R. China
[3] Department of Physics, Applied Physics, and Astronomy, Rensselaer Polytechnic Institute, Troy, New York 12180, USA
[4] Department of Materials Science and Engineering, Johns Hopkins University, Baltimore, Maryland 21218, USA
[5] State Key Laboratory of Silicon Materials, Department of Materials Sciences and Engineering, Zhejiang University, 38 Zheda Road, Hangzhou 310027, P. R. China

Received 15 June 2012, revised 21 August 2012, accepted 22 August 2012
Published online 27 September 2012

Dedicated to Stanford R. Ovshinsky on the occasion of his 90th birthday

**Keywords** GeSbTe, high resolution transmission electron microscopy, off-octahedral/tetrahedral Ge, radial distribution function

[*] Corresponding author: e-mail xqliu@bjut.edu.cn, Phone/Fax: +86-10-67392635
[**] e-mail xdhan@bjut.edu.cn, Phone/Fax: +86-10-67396087

Traditional Lorch-window technique was modified to the truncated Lorch-window through various truncation ranges to apply the Lorch-window functions. The terminal ripples in radial distribution functions (RDFs) were weakened and the shoulder peak at 2.6 Å in crystalline $Ge_2Sb_2Te_5$ (GST) was revealed by the indication of the off-octahedral Ge. The Cs-corrected high resolution transmission electron microscopy image and the corresponding simulations suggest that the off-octahedral Ge atoms are indeed in the tetrahedral symmetry. These results indicate that the complex structural details in the intermediate phase of GST other than simple rock-salt structure though the quantified information, such as the accurate atomic positions of the off-octahedral Ge need being further clarified in the future. These results also reveal the significance of high-Q signals in revealing the structures in short range order.

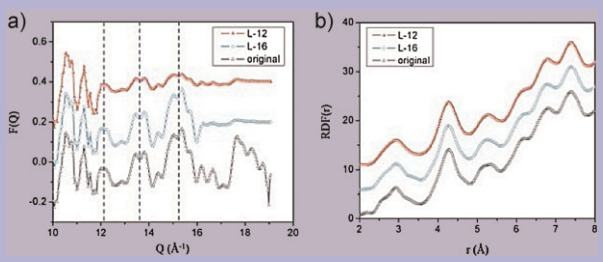


Left (a): Original reduced interference function $F(Q)$ (black) and truncated $F(Q)$ data. Right (b): Corresponding RDF curves. L-12 (red half-solid triangle) represent the data with a truncation range of 12 $Å^{-1}$, and L-16 (open square) for the truncation range of 16 $Å^{-1}$.



**1 Introduction** The $Ge_2Sb_2Te_5$ (GST) alloys, as the charming and successful phase-change materials [1], have been intensively investigated for more than two decades. The structural research is of great importance for secrete decoding in the phase change process. However, despite the intense efforts, the structure of the GST alloys has remained unclear, particularly the intermediate crystalline (meta-stable) phase [2–13].

The crystalline (*c*-) GST structure has been well studied by various techniques. These techniques can be classified into three groups: Rietveld refinement [3–6], full pair-distribution function (PDF) analyses [7–9], and imaging techniques [2, 11, 12]. However, the structure derived from these results still seems to be uncertain and confusing. The results of Rietveld refinement [3–6] indicate that the *c*-GST possesses a rocksalt-like (RS) structure. The Fourier-transformed EXAFS

spectra of the Ge and Te edges for *c*-GST [9] and the PDF analysis of *c*-GST [2, 10] both clearly show the existence of a shoulder peak at 2.6 Å, which could be a characteristic tetrahedral Ge (*t*-Ge), or at least, the off-octahedral Ge [2]. The imaging techniques, including traditional high resolution transmission electron microscopy (HRTEM), Cs-corrected HRTEM, and X-ray fluorescence holography (XFH) techniques, also propose the existence of *t*-Ge.

The structure of *c*-GST is distorted and complicated [2, 8–10]. Recently, Siegrist et al. [13] showed that depending on the annealing temperature, GST alloys had different degrees of disordering and thus very different resistance. Their findings further indicated the complexity of *c*-GST structure. Thus, a comprehensive understanding of the structure of *c*-GST is necessary, both for exploring the phase change mechanism and for understanding the relationship between the physical properties (optical and electrical) and the structures.

Here, through the way of modifying the Lorch-window method [14, 15] in PDF analysis to a truncated Lorch-window, combined with the Cs-corrected HRTEM image, we have verified the existence of off-octahedral Ge in *c*-$Ge_2Sb_2Te_5$ and further suggested that these off-octahedral Ge atoms could be in the tetrahedral positions. These results further demonstrate the significance of signals in high-$Q$ space in the structural analysis, especially structural details in the short range order.

**2 Experimental methods** $Ge_2Sb_2Te_5$ thin films about 20 nm in thickness are directly deposited onto the TEM grid with an ultrathin 5-nm-thick carbon film as a supporting layer. The GST thin film is deposited by rf magnetron sputtering using a GST alloy target and then annealed in a vacuum furnace for half an hour at 200 °C to obtain polycrystalline *c*-GST. The selected area electron diffraction experiments are performed on a JEOL-2010 TEM operated at 200 kV. The HRTEM experiments are done on a FEI Titan 80–300 TEM with a Cs corrector operated at 300 kV and the corresponding simulations are conducted by using the commercialized software Mactempas.

The conventional TEM images and corresponding diffraction patterns have been obtained and analyzed, showing that the samples with the nanoscaled poly-crystallines are the pure intermediate metastable phase of GST and no oxidation has been detected.

The diffraction intensity profiles are used to obtain the reduced interference function [16, 17]. The function $F(Q)$ is related to the reduced distribution function $G(r)$ by the Fourier transform as:

$$G(r) = \frac{2}{\pi}\int_0^{Q_{\max}} F(Q)\sin(Qr)\,\mathrm{d}Q. \quad (1)$$

The radial distribution function (RDF) is expressed as:

$$\mathrm{RDF}(r) = 4\pi r^2\rho + rG(r), \quad (2)$$

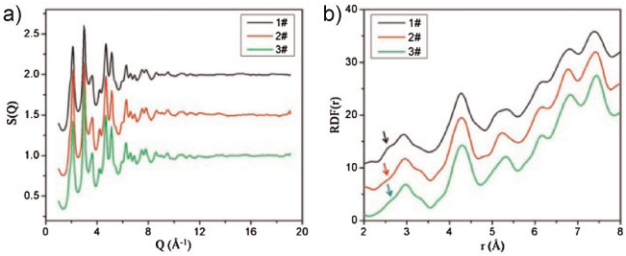


**Figure 1** (online color at: www.pss-b.com) (a) The structure factor $S(Q)$ obtained from three sets of independent diffraction data; (b) the corresponding RDFs.

where $Q$ is the scattering vector ($Q = 4\pi\sin\theta/\lambda$; $\theta$ is the half scattering angle; and $\lambda$ is the electron wavelength); $\rho$ is the average density of *c*-$Ge_2Sb_2Te_5$, about 0.033 atom Å$^{-3}$.

## 3 Results

**3.1 Original structure factor $S(Q)$ and corresponding RDFs** Figure 1a shows the raw structure factors $S(Q)$ from three sets of independent diffraction data. Figure 1b shows the corresponding RDFs, in which the 2.6 Å shoulders beside the 3.0 Å peak are indicated with arrows, clearly showing the existence of *t*-Ge in *c*-GST.

**3.2 The damping effect of the Lorch-window function and the exponential term** Ripples (below real structural features) arise from the Fourier transform due to the upper limit of the transform range [14–16, 18]. These ripples lower the reliability of the shoulder peak at 2.6 Å. To remove these terminal ripples in the PDFs, the Lorch-window function [14, 15] or a suitable exponential term [18–20] always be applied. This means that the interference function $F(Q)$ should be multiplied by a factor before the Fourier transformation. This factor is expressed as $Q_{\max}/(\pi Q)\sin(\pi Q/Q_{\max})$ ($Q_{\max}$ is the maximum $Q$-value in the experimental data) in the Lorch-window function, and it is expressed as $e^{-\alpha Q^2}$ ($\alpha$ is a constant, usually determined by the equation $e^{-\alpha Q_{\max}^2} = 0.1$) when the exponential term is applied. Figure 2a shows the change of the damping factors in the Lorch-window function and the exponential term ($\alpha = 0.0063$) along $Q$ space. The corresponding damped $F(Q)$ signals (after multiplying with the damping factor) and RDFs functions are shown in Fig. 2b and c, respectively. As shown in Fig. 2b, the $F(Q)$ signals in high $Q$ space, especially those beyond 12 Å$^{-1}$ are severely damped by the exponential term and Lorch-window function. The comparison of the corresponding RDFs shows that the 2.6 Å shoulder disappears in the damped RDFs (Fig. 2c). This means that the shoulder peak is very sensitive to the signals in high-$Q$ space (beyond 12 Å$^{-1}$) and the disappearance of the shoulder peak result from the dampening of the $F(Q)$ signals in the data processing for RDFs. Thus, to decide which part are real physical signals beyond 12 Å$^{-1}$, is critical to verify the existence of the 2.6 Å shoulder.

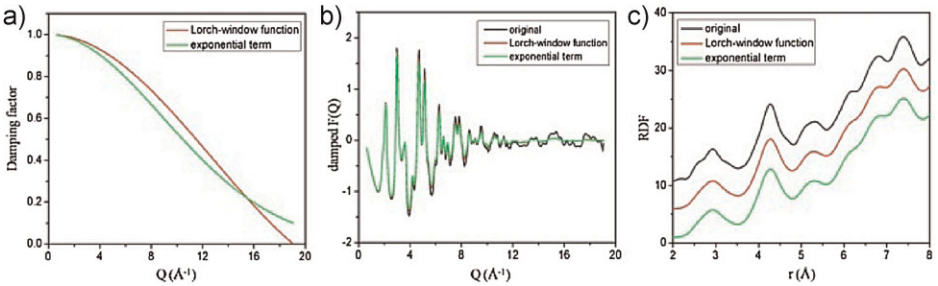


**Figure 2** (online color at: www.pss-b.com) (a) The damping factor in the Lorch-window function and exponential term ($\alpha = 0.0063$); (b) the corresponding damped $F(Q)$ and original $F(Q)$; and (c) the corresponding RDFs (Fourier transform of $F(Q)$).

**3.3 The real physical signals in high-$Q$ space** The damping factor is effective in removing the terminal ripples in PDFs and has been successful in the structural analysis of the amorphous phase for most cases. However, in the study for $c$-$Ge_2Sb_2Te_5$ intermediate phase, the damping factor should be used carefully because the crystalline phase usually possesses significant real physical signals in the high-$Q$ space, which can be damped by the Lorch-window function and the exponential term (Fig. 2b). Figure 3 magnifies the signals in Fig. 1a from 10 to 18 $Å^{-1}$ in $Q$ space. It is well known that the signal-noise ratio will be weakened in high-$Q$ space. Thus it is important to know which parts of the data are real signals. Figure 3 clearly shows that the signals below about 16 $Å^{-1}$ are well repeated through the three sets of data while those beyond 16 $Å^{-1}$ are non-repeatable. The repeatable signals (the light blue region in Fig. 3) are considered as the real physical signals. The unrepeatable signals are regarded as noises. The signals in high-$Q$ space (e.g., 12–16 $Å^{-1}$) correspond to the structural details in short range order and are extremely important and significant for revealing the structural details of the intermediate phase of $c$-$Ge_2Sb_2Te_5$.

**3.4 The application of the truncated Lorch-window functions** To eliminate the terminal effect (ripples), we use a truncated Lorch-window method. In this method, the real physical signals are kept unrevised (damping factor equals 1) while the noise parts in high-$Q$ space are modified by a Lorch-window function. Figure 4a shows the comparison of different truncation ranges, with the enlarged $Q$-range from 12 to 16 $Å^{-1}$ in the framed inset. The three apparent peaks indicated in the dotted lines are almost smeared out by the aggressive Lorch-window filtering with a truncation value of 12 $Å^{-1}$. Figure 4b compares the RDFs with different truncated ranges. The comparison shows that the ripples are noticeably weakened after the use of the truncated Lorch-window method. However, if a too aggressive truncation is used, some useful information can be filtered out. For example, the truncation of 12 $Å^{-1}$ may eliminate the shoulder peaks in the Fourier transform in Fig. 4b. The truncation of 16 $Å^{-1}$, in comparison, keeps the original signals, leading to the revelation of the presence of shoulders in the PDF. It is also noticeable in the RDFs from the original $F(Q)$ and truncated $F(Q)$ with the range of 16 $Å^{-1}$, that there is another clear existing shoulder above 3.0 Å, which has been generally attributed to the longer bonds in the distorted RS. This is also smeared out by the aggressive filtering with the truncation of 12 $Å^{-1}$. It further confirms that the shoulder peak at 2.6 Å is not due to the ripple effect.

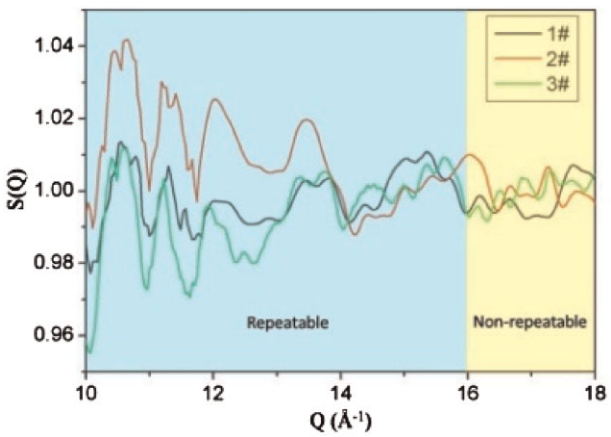


**Figure 3** (online color at: www.pss-b.com) The magnified $F(Q)$ in high-$Q$ space (10–18 $Å^{-1}$).

**3.5 The Cs-corrected HRTEM and the corresponding simulation techniques revealing the off-octahedral Ge atoms being in the tetrahedral positions in nanocrystalline $Ge_2Sb_2Te_5$** Through a series of careful analysis, we can conclude the significance of the high-Q signals (12–16 $Å^{-1}$) to reveal the existence of a shoulder peak at 2.6 Å, which is an indicator of the off-octahedral Ge. To further reveal the structural details of

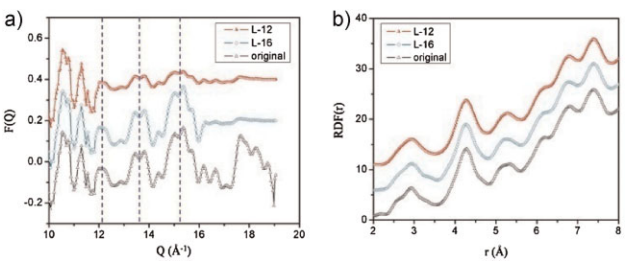


**Figure 4** (online color at: www.pss-b.com) (a) Original reduced interference function $F(Q)$ (black) and truncated $F(Q)$ data. (b) Corresponding RDF curves. L-12 (red half-solid triangle) represent the data with a truncation range of 12 $Å^{-1}$, and L-16 (open square) for the truncation range of 16 $Å^{-1}$.

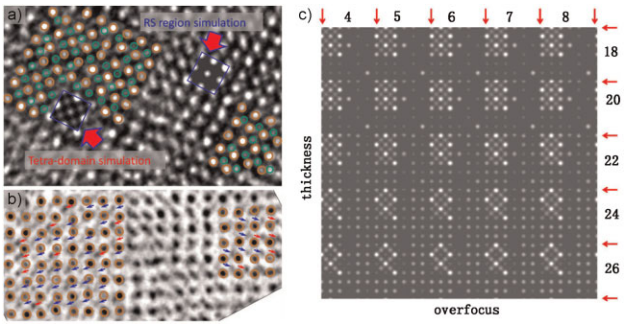


**Figure 5** (online color at: www.pss-b.com) (a) Cs-corrected HRTEM image showing off-octahedral Ge domains (circle-overlaid area) coexisting with RS regions. (b) Reprocessed HRTEM image in (a) by reversing the phases to show the off-octahedral Ge more clearly. In (a) and (b), the yellow circles represent Te atoms and the green circles represent off-octahedral Ge atoms. In (b), the red arrows indicate the strong spots in tetrahedral sites and the blue ones indicate the diffused and weak spots. (c) Systematic image simulations are based on the ideal (without distortion) of RS-V*t*GC-coexisted model for the sample thickness 18–26 nm and overfocus range 4–8 nm (the parameters we used in the experiment). Two selected typical simulated images are also over-laid with the octahedral domain and off-octahedral Ge domain (*t*-Ge) in (a), respectively.

the off-octahedral Ge, we have performed Cs-corrected HRTEM and corresponding multi-slice simulations. Figure 5a shows the Cs-corrected HRTEM image, which contains both the RS domains and the domains with the off-octahedral Ge (called V*t*GC domain by Ref. [2]). In Fig. 5a, the off-octahedral Ge domains are overlaid by yellow and green circles. The yellow circles represent Te atoms while the green circles represent off-octahedral Ge atoms. The distortions of both octahedral sites and tetrahedral sites in the off-octahedral Ge domains can be clearly observed in Fig. 5a. Also, in Fig. 5a, the two types of domains appear next to one another, thus excluding effects due to differences in sample thickness. Figure 5b shows the reprocessed HRTEM image in Fig. 5a by reversing the phases to show the off-octahedral Ge more clearly. In Fig. 5b, the red arrows indicate the strong spots in off-octahedral sites and the blue ones indicate the diffused and weak spots. The inhomogeneous spots intensity indicated by the red and blue arrows, combined the distortion of off-octahedral sites in off-octahedral domains, also prove that the off-octahedral Ge spots are not ghost images by the thickness effects.

From these atomic scale images, the off-octahedral Ge can be suggested to be in the tetrahedral positions (*t*-Ge), agreeing well with the results of V*t*GC model [2, 25]. Systematic image simulations based on the ideal (without distortion) of RS-V*t*GC-coexisted [2] model have been performed and shown in Fig. 5c, for the sample thickness (18–26 nm) and defocus parameters we used in the experiment. For the RS structure, no ghost spots appear at tetrahedral sites under all simulation conditions. In contrast, when V*t*GC domains [2] are added into the simulation model, the off-octahedral Ge (*t*-Ge) spots appear in the over-focus range of 4–8 nm. Two selected typical simulated images are also over-laid with the octahedral domain and tetrahedral domain in Fig. 5a, respectively. The direct comparison strongly suggests the presence of atoms in tetrahedral sites.

**4 Discussion** According to the Gaussian peak splitting method used by Liu et al. [2], the fraction of *t*-Ge can be coarsely evaluated to be one-third of the total Ge. During the far-from-equilibrium, laser-induced rapid phase transition in a real device, it is unlikely that the RS state is the only structure obtained for *c*-GST, given that the timescale available for crystallization is limited to nanoseconds. Therefore, information about other structural variations, including those with limited metastability, should be of practical importance. This is especially relevant because the optical properties, according to the previous calculations, exhibit little difference among these crystalline states [2]. It seems reasonable from kinetic considerations that some of the tetrahedrally bonded Ge, known to constitute approximately one-third of all the Ge atoms in the parent amorphous GST [11], are retained such that the *c*-GST involving some left-over *t*-Ge is the first configuration to reach, thereby leading to intermediate metastable states, into which the amorphous GST is crystallize. This may further help to explain the rapid phase change observed, since the transition (and the optical contrast) does not require that all of the tetrahedrally bonded Ge atoms in the amorphous state transform to the octahedral sites upon crystallization in one quick step.

The existence of significant amount of off-octahedral Ge in the *c*-GST phase and the related coherent domain structure have been noticed by several groups [2, 22]. This structural picture is consistent with the variation of electrical properties in the crystalline phase derived from the local charge carrier difference of the off-octahedral Ge and the averaged octahedral structural framework.

Some studies have proposed that the off-octahedral Ge is indeed, located at tetrahedral positions in the nanocrystalline GST intermediate phase [2, 21] while others suggest a picture of local-disordering arrangement of Ge atoms [22]. The tetrahedral and disordered Ge are energetically slightly higher than octahedral Ge in the RS-based structural framework of GeSbTe alloys, it is possible for us to capture such a metastable state between the amorphous and the equilibrium crystalline phases, especially in the nanocrystalline phases, where such sites are present. However, uncertainties still exist [21–28], and further efforts are necessary to give accurate descriptions of the off-octahedral Ge to be tetrahedral Ge or distorted-tetrahedral Ge or even localized disordered Ge.

**5 Conclusions** Combining a truncated Lorch-window method, we have revealed the existence of off-octahedral Ge in nanocrystalline GST and also discovered the significance of high-Q signals in revealing the structural details in short range order. Further Cs-corrected HRTEM and the

corresponding simulation techniques suggest that the off-octahedral Ge atoms are in the tetrahedral positions. Since TEM techniques used here do not provide the bonding natures of the off-octahedral Ge, to unambiguously conclude the exact position of off-octahedral Ge (e.g., whether they are the *t*-Ge atoms), more efforts are necessary, especially those element specific techniques, or combined ones.

**Acknowledgements** This work was supported by the National Basic Research Program of China (2009CB623700) and Beijing Natural Science Foundation (1122003).

## References

[1] S. R. Ovshinsky, Phys. Rev. Lett. **21**, 1450 (1968).
[2] X. Q. Liu, X. B. Li, L. Zhang, Y. Q. Cheng, Z. G. Yan, M. Xu, X. D. Han, S. B. Zhang, Z. Zhang, and E. Ma, Phys. Rev. Lett. **106**, 025501 (2011).
[3] E. T. Kim, J. Y. Lee, and Y. T. Kim, Appl. Phys. Lett. **91**, 101909 (2007).
[4] S. Hosokawa, T. Ozaki, K. Hayashi, N. Happo, M. Fujiwara, K. Horii, P. Fons, A. V. Kolobov, and J. Tominaga, Appl. Phys. Lett. **90**, 131913 (2007).
[5] T. Matsunaga, N. Yamada, and Y. Kubota, Acta Crystallogr. B **60**, 685 (2004).
[6] T. Matsunaga, R. Kojima, N. Yamada, K. Kifune, Y. Kubota, Y. Tabata, and M. Takata, Inorg. Chem. **45**, 2235 (2006).
[7] T. Matsunaga, H. Morita, R. Kojima, N. Yamada, K. Kifune, Y. Kubota, Y. Tabata, J.-J. Kim, M. Kobata, E. Ikenaga, and K. Kobayashi, J. Appl. Phys. **103**, 093511 (2008).
[8] T. Nonaka, G. Ohbayashia, Y. Toriumi, Y. Mori, and H. Hashimoto, Thin Solid Films **370**, 258 (2000).
[9] A. Kolobov, P. Fons, A. I. Frenkel, A. L. Ankudinov, J. Tominaga, and T. Uruga, Nature Mater. **3**, 703 (2004).
[10] S. Shamoto, N. Yamada, T. Matsunaga, Th. Proffen, J. W. Richardson, J.-H. Chung, and T. Egam, Appl. Phys. Lett. **86**, 081904 (2005).
[11] M. Xu, Y. Q. Cheng, H. W. Sheng, and E. Ma, Phys. Rev. Lett. **103**, 195502 (2009).
[12] S. Kohara, K. Kato, S. Kimura, H. Tanaka, T. Usuki, K. Suzuya, H. Tanaka, Y. Moritomo, T. Matsunaga, N. Yamada, Y. Tanaka, H. Suematsu, and M. Takata, Appl. Phys. Lett. **89**, 201910 (2006).
[13] T. Siegrist, P. Jost, H. Volker, M. Woda, P. Merkelbach, C. Schlockermann, and M. Wuttig, Nature Mater. **10**, 202 (2011).
[14] E. Lorch, J. Phys. C **2**, 229 (1969).
[15] M. Tewes, J. Zweck, and H. Hoffmann, J. Phys.: Condens. Matter **6**, 835 (1994).
[16] N. E. Cusack, The Physics of Structurally Disordered Matter: An Introduction (Adam Hilger, Bristol, 1987), pp. 55–81.
[17] T. Ohkatsu and Y. Hirotsu, Phys. Rev. B **67**, 094201 (2003).
[18] D. R. Mckenzie, L. C. Botten, and R. C. Mcphedran, Phys. Rev. Lett. **51**, 4 (1983).
[19] P. D'Antonio, C. George, A. H. Lowrey, and J. Karle, J. Chem. Phys. **55**, 1071 (1971).
[20] J. H. Konnert and J. Karle, Acta Cryst. A **29**, 702 (1973).
[21] S. Sen, T. G. Edwards, J.-Y. Cho, and Y.-C. Joo, Phys. Rev. Lett. **108**, 195506 (2012).
[22] M. Krbal, A. V. Kolobov, P. Fons, and J. Tominaga, Phys. Rev. B **86**, 045212 (2012).
[23] P. Fons, A. V. Kolobov, J. Tominaga, S. Kohara, M. Takata, T. Matsunaga, N. Yamada, and S. Bokoch, Phys. Rev. Lett. **108**, 239603 (2012).
[24] J. Y. Raty, C. Bichara, R. Mazzarello, P. Rausch, P. Zalden, and M. Wuttig, Phys. Rev. Lett. **108**, 239601 (2012).
[25] X. Q. Liu, X. B. Li, L. Zhang, Y. Q. Cheng, Z. G. Yan, M. Xu, X. D. Han, S. B. Zhang, Z. Zhang, and E. Ma, Phys. Rev. Lett. **108**, 239602 (2012).
[26] M. Upadhyay, S. Murugavel, M. Anbarasu, and T. R. Ravindran, J. Appl. Phys. **110**, 083711 (2011).
[27] T. G. Edwards, E. L. Gjersing, S. Sen, S. C. Currie, and B. G. Aitken, J. Non-Cryst. Solids **357**, 3036 (2011).
[28] S. Hosokawa, W. Pilgrim, A. Höhle, D. L. Szubrin, N. Boudet, J. Bérar, and K. Maruyama, J. Appl. Phys. **111**, 083517 (2012).

 